Five gaps Eliashberg model for KCa2Fe4As4F2: relevance of the electronic band

# Five gaps Eliashberg model for $KCa_2Fe_4As_4F_2$: relevance of the electronic band

Giovanni Ummarino[a], Daniele Torsello[b,*]

[a]*Dipartimento di Scienza Applicata e Tecnologia, Politecnico di Torino, Corso Duca degli Abruzzi 24, 10129 Torino, Italy*
*National Research Nuclear University MEPhI (Moscow Engineering Physics Institute), Kashira Hwy 31, Moskva 115409, Russia*
[b]*Dipartimento di Scienza Applicata e Tecnologia, Politecnico di Torino, Corso Duca degli Abruzzi 24, 10129 Torino, Italy*
*Istituto Nazionale di Fisica Nucleare - Sezione di Torino, Via Pietro Giuria 1, 10125 Torino, Italy*

**Abstract**

Experimental data from the recently discovered iron-based superconductor (IBS) $KCa_2Fe_4As_4F_2$ is analyzed within a realistic five-band $s_\pm$ Eliashberg model with coupling provided by antiferromagnetic spin fluctuations. Fundamental parameters are deduced from available angle resolved photoemission spectoscopy (ARPES) and ab-initio density functional theory (DFT) data, and several physical properties are calculated: critical temperature, upper critical field, gap values, resistivity and superfluid density. This procedure, usually extremely successful in IBSs, highlights the peculiar behavior of this new compound in which $s$ and $d$ -wave character might coexist and where the electron band is close to vanish.

*Keywords:* Eliashberg theory, Iron based superconductors, multigap superconductivity, multiband superconductor.

## 1. Introduction

Eliashberg theory gives powerful tools for the understanding of the fundamental properties of newly discovered materials whose characteristics go beyond the standard BCS model (1; 2; 3; 4). Iron based superconductors (IBSs) are characterized by multiple bands crossing the Fermi surface, resulting in multiple Fermi sheets on which the superconducting gaps open (5). A large consensus was established on antiferromagnetic spin fluctuations (AFM-SF) being the main responsible for pairing in these materials, with other mechanisms (orbital fluctuations, phonons, nematicity) playing a minor role (6; 7; 8; 9). This repulsive coupling can support superconductivity if the order parameters on the regions of the Fermi surface that are coupled have opposite signs. This is the case for both $d$-wave gaps and for the $s_\pm$ picture that was identified in most IBSs (10; 11). The typical Fermi surface (FS) of these materials involves both hole pockets at the center of the Brillouin zone and electron pockets at the $M$ or $X$ point (12). The number and size of these pockets depends on the stoichiometry of the specific compound, as do the fine details of their shape, despite they all roughly share the same qualitative structure.
In this frame, $KCa_2Fe_4As_4F_2$ stands out for some peculiarities. Angle resolved photoemission spectoscopy (ARPES) experiments (13) and ab-initio density functional theory (DFT) calculations (14; 15) both showed very small electron pockets at the $M$ point, almost reminding the situation of $KFe_2As_2$ where only hole pockets survive (7). Moreover, the possible presence of lines of nodes (compatible with $d$-wave superconductivity) was suggested due to the shape of the superfluid density measured by $\mu$SR (16) and by low temperature specific heat features (17).
These features might stem from the very anisotropic nature of this compound (belogning to the new "12442" IBS family (18; 19; 20)), whose structure resembles that of cuprates for many aspects. The Fe-As layers that support superconductivity are widely spaced by insulating $Ca_2F_2$ blocks (21), bilayer splitting effects was observed (13), and resistivity (22), critical fields (23) and London penetration depth show very large anisotropy. The importance of the spacer layers in the determination of the superconducting properties of IBSs stems from both its thickness (24), and from its chemical nature(25).
For all these reasons, applying the typical Eliashberg approach that has been so successful in other IBSs families (26; 27; 28; 29) can be very instructive: one could expect some features to be well reproduced, but some failures of the model should emerge, shedding light on the peculiarities of $KCa_2Fe_4As_4F_2$. In this paper, we employ the most realistic Eliashberg $s_\pm$ model (described in Sect. 2) with pairing parameters deduced by ARPES (13) and DFT data (15) to calculate critical temperature, upper critical field, gap values, resistivity and superfluid density. The obtained values and behaviors are compared in Sect. 3 to experimental data from the literature, and discussed in terms of the peculiar features of this material. In Sect. 4 conclusions on the fundamental properties and peculiarities of $KCa_2Fe_4As_4F_2$ are finally drawn.

## 2. Eliashberg model

High-resolution laser-based ARPES measurements on single crystals of $KCa_2Fe_4As_4F_2$ identified five hole Fermi surface sheets around the $\Gamma$ point, and very small electron pockets around the $M$ point (13). Two pairs of hole FSs are the result of bilayer splitting due to interlayer interorbital interaction

*Corresponding author.
*Email address:* daniele.torsello@polito.it (Daniele Torsello)

between the two FeAs layers in a bilayer block. The order parameters measured on the outermost pair are extremely close, yielding two practically identical bands that can be summed up in the Eliashberg model (30; 31) to yield a total of four equivalent hole bands and one electron band.

Therefore, in the $s_{\pm}$-wave picture the five-band Eliashberg theory consist of a set of 10 coupled equations for the five gaps $\Delta_i(i\omega_n)$ and five renormalization functions $Z_i(i\omega_n)$ to be solved self-consistently (32; 33; 27). On the imaginary-axis, neglecting disorder-induced scattering and Coulomb pseudopotentials that are close to zero in clean IBSs, the isotropic equations read:

$$\omega_n Z_i(i\omega_n) = \omega_n + \pi T \sum_{m,j} \Lambda^Z_{ij}(i\omega_n, i\omega_m) N^Z_j(i\omega_m) \tag{1}$$

$$Z_i(i\omega_n)\Delta_i(i\omega_n) = \pi T \sum_{m,j} [\Lambda^{\Delta}_{ij}(i\omega_n, i\omega_m)] \times \Theta(\omega_c - |\omega_m|) N^{\Delta}_j(i\omega_m) \tag{2}$$

Here $i$ is a band index ranging from 1 to 5, $\omega_n$ are the Matsubara frequencies, $\Lambda^Z_{ij}(i\omega_n, i\omega_m) = \Lambda^{ph}_{ij}(i\omega_n, i\omega_m) + \Lambda^{sf}_{ij}(i\omega_n, i\omega_m)$ and $\Lambda^{\Delta}_{ij}(i\omega_n, i\omega_m) = \Lambda^{ph}_{ij}(i\omega_n, i\omega_m) - \Lambda^{sf}_{ij}(i\omega_n, i\omega_m)$, where

$$\Lambda^{ph,sf}_{ij}(i\omega_n, i\omega_m) = = 2\int_0^{+\infty} d\Omega \Omega \alpha^2_{ij} F^{ph,sf}(\Omega)/[(\omega_n - \omega_m)^2 + \Omega^2]. \tag{3}$$

$\Theta$ is the Heaviside function and $\omega_c$ is a cutoff energy. The superscript $sf$ indicates the spin-fluctuations frequency dependent spectral function $\alpha^2_{ij}F(\Omega)$ while $ph$ the phononic one, both considered to have a Lorentzian shape:

$$\alpha^2_{ij}F^{sf,ph}(\Omega) = C_{ij}\{L(\Omega + \Omega_{ij}, Y_{ij}) - L(\Omega - \Omega_{ij}, Y_{ij})\},$$

where

$$L(\Omega \pm \Omega_{ij}, Y_{ij}) = \frac{1}{(\Omega \pm \Omega_{ij})^2 + Y^2_{ij}}$$

and $C_{ij}$ are normalization constants, necessary to obtain the proper values of $\lambda_{ij}$, while $\Omega_{ij}$ and $Y_{ij}$ are the peak energies and the half-widths of the Lorentzian functions, set to be $\Omega_{ij} = \Omega_0$ and $Y_{ij} = \Omega_0/2$, based on the results of inelastic neutron scattering measurements (34).

Moreover, $N^{\Delta}_j(i\omega_m) = \Delta_j(i\omega_m)/\sqrt{\omega^2_m + \Delta^2_j(i\omega_m)}$ and $N^Z_j(i\omega_m) = \omega_m/\sqrt{\omega^2_m + \Delta^2_j(i\omega_m)}$. Finally, the electron-boson coupling constants are defined as $\lambda^{sf,ph}_{ij} = 2\int_0^{+\infty} d\Omega \frac{\alpha^2_{ij}F^{sf,ph}(\Omega)}{\Omega}$.

### 2.1. Input parameters

The value of representative antiferromagnetic spin fluctuaction energy $\Omega_0$ is known and it is equal to 16 meV (21). Considering all the approximations discussed above (pairing provided mainly by SF, isotropic gaps, 5 bands of which 1 with electron character, negligible scattering) we are left with a $5 \times 5$ coupling constant matrix. Fortunately, the nature of IBSs allows to largely simplify the matrix (27). We put all diagonal components (phononic) equal to 0.1 because the total electron-phonon coupling in pnictides is generally small (35) and phonons mainly provide intraband coupling, while the AFM-SF pairing is only interband (36). Moreover, not all bands are coupled to each other, but only those crossing the Fermi level at different points of the Brillouin zone: $\Gamma$ and $M$. Therefore only the electron pocket (band 5) will be coupled to all hole bands, and no other coupling parameter is $\neq 0$.

Finally, symmetric contributions such as $\Lambda_{ij}$ and $\Lambda_{ji}$ are related to each other through density of states (DOS) ratio on the two bands ($\nu_{ij} = N_i(0)/N_j(0)$, where $N_i(0)$ is the normal density of states at the Fermi level for the $i$-th band) that can be estimated from the size of the Fermi surface calculated by DFT (37; 38). The resulting coupling matrix is therefore the following:

$$\Lambda_{ij} = \begin{pmatrix} 0.1 & 0 & 0 & 0 & \lambda^{sf}_{15} \\ 0 & 0.1 & 0 & 0 & \lambda^{sf}_{25} \\ 0 & 0 & 0.1 & 0 & \lambda^{sf}_{35} \\ 0 & 0 & 0 & 0.1 & \lambda^{sf}_{45} \\ \lambda^{sf}_{15}\nu_{15} & \lambda^{sf}_{25}\nu_{25} & \lambda^{sf}_{35}\nu_{35} & \lambda^{sf}_{45}\nu_{45} & 0.1 \end{pmatrix} \tag{4}$$

Where the four coupling elements ($\lambda^{sf}_{15}$,$\lambda^{sf}_{25}$,$\lambda^{sf}_{35}$,$\lambda^{sf}_{45}$) are the only free parameters of the model, fixed to reproduce at best the experimental critical temperature and gap values. Once this is done, all other physical properties can be computed.

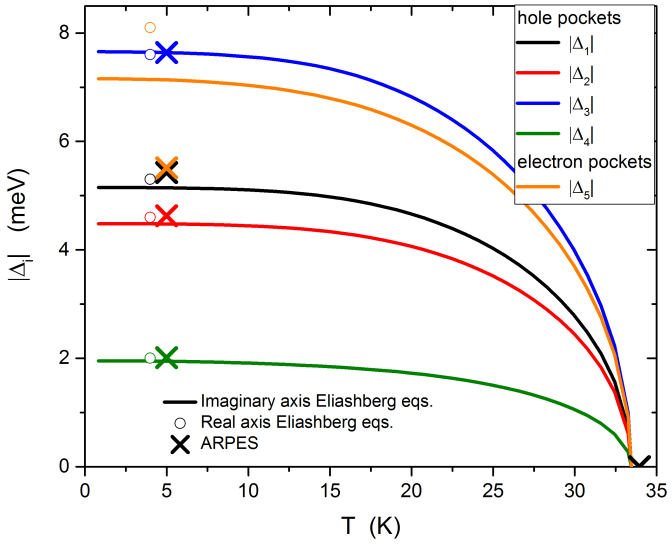


Figure 1: Temperature dependence of the five gaps values calculated from imaginary axis Eliashberg equations (solid lines). The experimental values of the gaps from ARPES measurements (13) are shown as crosses and can be compared with the values from the analytical continuation of the imaginary axis solutions of the Eliashberg equations on the real axis (open symbols) obtained with the Padé approximants approach.

## 3. Comparison with experimental data

### *3.1. Superconducting state properties*

Figure 1 shows the gap values and critical temperature (where all gaps vanish) calculated in the five-band Eliashberg model compared to the experimental data from ARPES measurement (13). The coupling parameters employed to obtain these values are shown in Table 1 together with the DOS ratios extracted from ab-initio calculations in Ref. (15).

Table 1: Input parameters for the Eliashberg model: $\lambda_{ij}^{sf}$ are the coupling matrix elements, $\nu_{ij}$ the DOS ratios deduced from (15).

| bands $i$, $j$ | $\lambda_{ij}^{sf}$ | $\nu_{ij}$ |
|---|---|---|
| 1, 5 | 1.10 | 0.067 |
| 2, 5 | 0.65 | 0.170 |
| 3, 5 | 2.31 | 0.203 |
| 4, 5 | 0.24 | 0.285 |

The total average electron-boson coupling constant in the superconductive state is $\lambda_{s,tot} = 1.59$, indicating a moderately strong coupling with respect to other iron compounds (33). The critical temperature value found is exactly equal to the experimental one in the ARPES data and perfectly in the range usually reported for $KCa_2Fe_4As_4F_2$. Overall, also the calculated gap values are satisfactorily close to the experimental ones. Interestingly, the band on which the worst agreement with experimental data is found is the electron one. However, not much can be done to bring it closer to the experimental values since all hole bands are coupled to this band, and therefore contribute to the strength of superconductivity on this FS: a better agreement could be achieved only at the expense of a strong decrease of $T_c$. This can be interpreted as a first warning of the great relevance of the very small electronlike band in the determination of the properties of this compound.

Once the five gaps and renormalization functions have been calculated, it is possible to compute observable properties and their temperature dependencies.

For the calculation of the upper critical field $B_{c2}$, the linearized gap equations in the presence of a magnetic field can be solved (40; 26):

$$\omega_n Z_i(i\omega_n) = \omega_n + \pi T \sum_{m,j} \Lambda_{ij}(i\omega_n - i\omega_m)\mathrm{sign}(\omega_m)$$

$$Z_i(i\omega_n)\Delta_i(i\omega_n) = \pi T \sum_{m,j} [\Lambda_{ij}(i\omega_n - i\omega_m)] \cdot \cdot\theta(|\omega_c| - \omega_m)\chi_j(i\omega_m)Z_j(i\omega_m)\Delta_j(i\omega_m)$$

$$\chi_j(i\omega_m) = (2/\sqrt{\beta_j}) \int_0^{+\infty} dq \exp(-q^2) \cdot \cdot \tan^{-1}\left[\frac{q\sqrt{\beta_j}}{|\omega_m Z_j(i\omega_m)| + i\mu_B H_{c2}\mathrm{sign}(\omega_m)}\right]$$

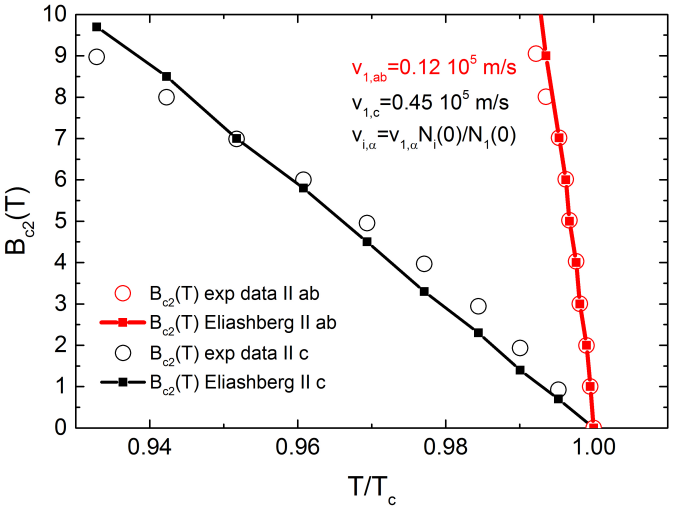


Figure 2: Comparison of the calculated and experimental (from Ref. (39)) upper critical field in the in-plane and out-of-plane configurations.

Here one additional parameter enters in the calculation. The expression $\beta_j = \pi H_{c2} v_{Fj}^2/(2\Phi_0)$, depends on the bare Fermi velocities $v_{Fj}$ of each band. However, within the same approximation of the free-electron gas already employed, $v_{Fi} \propto N_i(0)$ so that $v_{Fk} = \nu_{k1} v_{F1}$ for $k \in [2,5]$ (26). Therefore the only new free parameter is $v_{F1}$, that will have different values depending on the direction of the applied field: parallel to the $c$ axis or to the $ab$ plane. We find that the best fit of the experimental data (shown in Fig. 2) is obtained with a $v_F$ anisotropy ($v_{F1c}/v_{F1ab}$) close to 3.75: $v_{F1c} = 0.45 \cdot 10^{-5}$ m/s and $v_{F1ab} = 0.12 \cdot 10^{-5}$ m/s. A very good agreement with experimental data (39) is found for a magnetic field applied in plane, and an acceptable one is found also for out of plane fields.

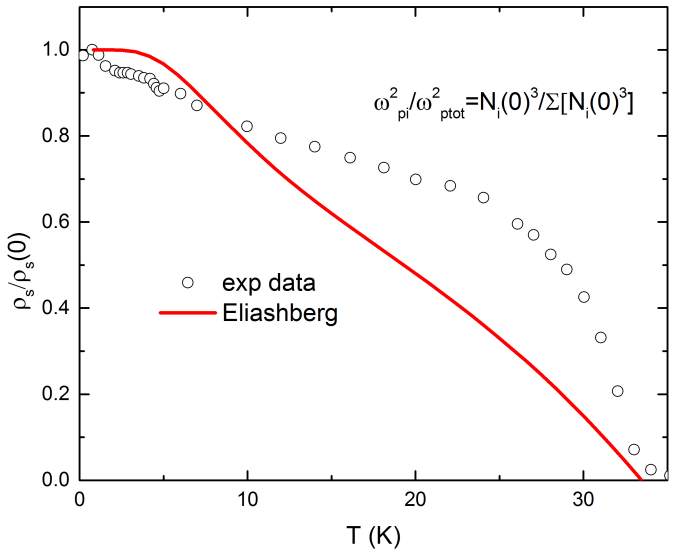


Figure 3: Comparison of the calculated and experimental (from Ref. (16)) temperature dependence of the superfluid density.

The temperature dependence of the superfluid density can

also be computed starting from the obtained gaps and renormalization functions (41). Each band contributes to the total density with a mixing weight (related to the plasma frequency of each band $w_i^\lambda = \omega_{p,i}^2/\omega_{p,tot}^2$) (42) that can be very roughly approximated to $w_i^\lambda \sim N_i(0)^3/(\sum_i N_i(0)^3)$ as in the free electron model:

$$\lambda^{-2}(T) = (\frac{\omega_{p,tot}}{c})^2 \sum_{i=1}^{3} w_i^\lambda \pi T \times \sum_{n=-\infty}^{+\infty} \frac{\Delta_i^2(\omega_n) Z_i^2(\omega_n)}{[\omega_n^2 Z_i^2(\omega_n) + \Delta_i^2(\omega_n) Z_i^2(\omega_n)]^{3/2}} \quad (5)$$

The results are shown in Fig. 3 where they are compared to $\mu$SR data (16). This comparison is particularly instructive since the superfluid density can give important indications about the presence of nodes and the symmetry of the order parameter (5). Interestingly, we obtain a quite different behavior, although some qualitative similarities can be found. Both the experimental and calculated data deviate largely from the typical BCS behavior and resemble the superposition of two separate behaviors at lower and higher temperatures (5). However, the $\mu$SR data has a much steeper increase of $\rho_s$ just below $T_c$ followed by a strong flattening of the curve between $\sim$ 15 and $\sim$ 25 K. The low temperature linear increase of $\rho_s$ with decreasing T was interpreted as an indication that $d$-wave superconductivity might play a role (16): the best fit for the data proposed by the authors yielded a large $s$-wave gap ($\Delta_s$ = 10.12 meV) and a small $d$-wave gap ($\Delta_d$ = 1.84 meV). Clearly, this can not be ruled out by our data, but we warn that unusual temperature dependencies of the superfluid density might also originate from the fine details of the small electron pockets that are crucial for the SF pairing, by a superposition of small gaps contributions (very non BCS behavior are strongly influenced by small gaps with high DOS (43)), and (as suggested in a very similar case (44)) from secondary magnetic phases contribution. It should also be noted that the poor agreement between calculated and experimental data is not determined by the free-electron approximation employed to estimate $w_i^\lambda$: even considering these parameters as free the experimental behavior could not be recovered.

### *3.2. Normal state properties*

Moreover, also normal state properties can be computed with an approach consistent with the Eliashberg one employed for the superconducting state. The resistivity in a multiband system can be obtained considering the contribution of all the different channels in an extension of the single band case (45; 46)

$$\rho(T) = \left( \frac{\varepsilon_0(\hbar\omega_p))^2}{\hbar} \sum_{i=1}^{N} \frac{(\omega_{p,i}/\omega_p)^2}{\gamma_i + W_i(T)} \right)^{-1}, \quad (6)$$

where $N$ is the total number of the different channels considered and $\gamma_i$ is the sum of the inter- and intra-band non magnetic and magnetic impurity scattering rates that are in principle present in the Eliashberg equations. It should be noted that in our Eliashberg model we neglected these scattering contributions for two reasons: the interband scattering rates are the ones affecting the superconducting properties and are negligible in clean pristine single crystals as the ones considered here, whilst the intraband ones, that are predominant in determining the residual resistivity, do not affect the superconducting properties. Finally

$$W_i(T) = 4\pi k_B T \int_0^\infty d\Omega \left[ \frac{\hbar\Omega/2k_BT}{\sinh(\hbar\Omega/2k_BT)} \right]^2 \frac{\alpha_{tr,i}^2 F_{tr}(\Omega)}{\Omega}, \quad (7)$$

with

$$\alpha_{tr,i}^2 F_{tr}(\Omega) = \sum_{j=1}^{N} \alpha_{tr,ij}^2 F_{tr}(\Omega), \quad (8)$$

where $\alpha_{tr,ij}^2(\Omega)F_{tr}(\Omega)$ are the transport spectral functions, that in the phononic case are directly related to the Eliashberg functions (47).

As in the superconductive state, we set all the spectral functions to be equal and to differ just for a scaling factor, the coupling constant ($\lambda_{tr,ij}$, defined as in Eliashberg Theory (47).), then $\alpha_{tr,i}^2 F_{tr}(\Omega) = \lambda_{tr,i}\alpha_{tr}^2 F'_{tr}(\Omega)$ and $\lambda_{tr,i} = \sum_{j=1}^{N} \lambda_{tr,ij}$.

The specific shape of the spectral function for the antiferromagnetic spin fluctuation in the normal state is different from the ones employed in the superconductive state (47), in particular for the behavior for $\Omega \to 0$, where the transport function behaves like $\Omega^3$ instead of $\Omega$. Therefore, the condition $\alpha_{tr}^2(\Omega)F_{tr}(\Omega) \propto \Omega^3$ should be imposed in the range $0 < \Omega < \Omega_D$, with $\Omega_D \approx \Omega_0/10$ where $\Omega_0$ is the representative bosonic energy (47). Then $\alpha_{tr}^2(\Omega)F'_{tr}(\Omega) = b_i\Omega^3\vartheta(\Omega_D - \Omega) + c_i\alpha_{tr}^2(\Omega)F''_{tr}(\Omega)\vartheta(\Omega - \Omega_D)$ and the constants $b_i$ and $c_i$ have been fixed by requiring the continuity in $\Omega_D$ and the normalization.

In order to describe the coupling with spin fluctuations we chose for the $\alpha_{tr}^2(\Omega)F''_{tr}(\Omega)$ the functional form of the theoretical antiferromagnetic spin fluctuations function in the normal state (31) that reproduces the experimental data concerning the normal state dynamical spin susceptibility (34)

$$\alpha_{tr}^2 F''(\Omega) \propto \frac{\Omega_0\Omega}{\Omega^2 + \Omega_0^2}\vartheta(\Omega_c - \Omega), \quad (9)$$

where $\Omega_c$ is a cut-off energy (in these calculations $\Omega_c$ = 1 eV) and $\Omega_0$ is the energy of the peak.

When, as in this case, the Fermi surface presents several sheets, a multi-band model is necessary to explain also the normal state properties. However, here the predominant feature is the holonic or electronic character of the carrier. Therefore it is sufficient to group together all the hole and the electron bands (separately), leaving a model containing only two different kind of carriers. Within this model, the electron-boson coupling constants $\lambda_{1,tr}$ and $\lambda_{2,tr}$, the impurities contents $\gamma_1$ and $\gamma_2$, the plasma energies $\omega_{p,1}$ and $\omega_{p,2}$, the representative energy $\Omega_0$ of the transport electron-boson spectral functions and the energy $\Omega_D$ are free parameters. Since the materials of the 12442 family are hole doped materials, a weaker electron mobility is expected (48). This means that within our model the impurities are mostly concentrated in the electron band (indicated by the index 2), i.e. $\gamma_2 \gg \gamma_1$, and the transport coupling is much

higher in the hole band (49). In this way one contribution results to be almost temperature independent and the other changes the slope of the resistivity with the temperature. In the equation for the resistivity just the rates $\left(\frac{\omega_{p,1}}{\omega_p}\right)^2$ and $\left(\frac{\omega_{p,2}}{\omega_p}\right)^2 = 1 - \left(\frac{\omega_{p,1}}{\omega_p}\right)^2$ play a role, therefore reducing the number of free parameters. We find $\lambda_{1,tr} = 1.30$, $\lambda_{2,tr} = 0.10$ ($\lambda_{tr,tot} = 0.95$), $\gamma_1 = 1$ meV, $\gamma_2 = 195$ meV, $\left(\frac{\omega_{p,1}}{\omega_p}\right)^2 = 0.277$ $\Omega_0 = 25$ meV and we choose, as usual (47), $\Omega_D = \Omega_0/10$. We can note that there is a increase of the typical energy $\Omega_0$ of the electron-boson coupling from the superconducting to the normal state in agreement with inelastic neutron scattering experimental data (34) and a significant decrease of the coupling constant $\lambda_{tot}$. This behavior is typical of cuprates (48) and iron-based materials (50; 51) although here the differences are not as large. From this point of view this material behaves less "unconventionally". Finally, Fig. 4 shows an excellent agreement of the computed and experimental ((13)) resistivity, indicating that normal state properties are less affected by the small details of the electronic structure, especially if related to the electron band that has a minor role in the normal state transport.

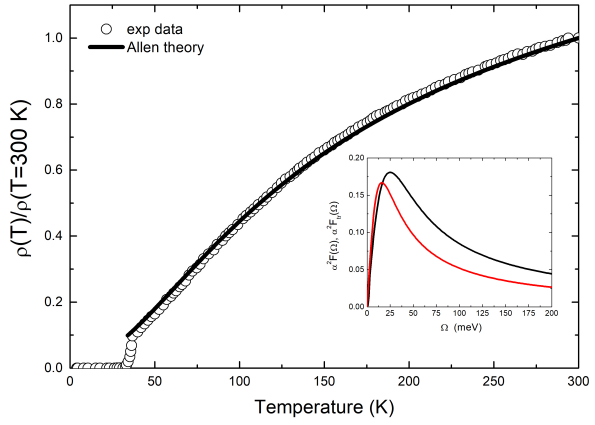


Figure 4: Comparison of the calculated and experimental (from Ref. (13)) normalized resistivity. The inset shows the AFM-SF spectral functions in the superconducting and normal states.

## 4. Conclusions

In conclusion, a five-band $s_{\pm}$ Eliashberg model for the properties of $KCa_2Fe_4As_4F_2$ was implemented and analyzed. This approach, usually able to nicely reproduce all experimentally observed features of IBSs, in this case is able to interpret most experimental data ($T_c$, gap values on the hole bands, upper critical fields, normal state resistivity) but highlights for this material two critical aspects, that we attribute to features specific of this system. In particular: the value of the gap on the electronic band is overestimated and the experimental temperature dependence of the superfluid density cannot be reproduced. We ascribe the former to the fact that fine details of the very small pockets play an important role in the determination of the gap values. Regarding the latter, the presence of $d$-wave superconductivity represents one possible explanation. However, we warn the reader that here the situation is complicated by the multiband nature of $KCa_2Fe_4As_4F_2$, were low temperature behavior could also be determined by small gaps with high DOS. Finally, the fact that features that are less affected by the fine details of the small electron pockets (such as the normal state resistance, $T_c$, and upper critical fields) are obtained in the model nicely agreeing with experiment, indicate that this system shares the major features typical of IBSs.

## Acknowledgments

G.U. acknowledges support from the MEPhI Academic Excellence Project (Contract No. 02.a03.21.0005), D.T. was partially supported by the Italian Ministry of Education, University and Research (Project PRIN "HIBiSCUS", Grant No. 201785KWLE). Both authors thank Gianluca Ghigo for useful discussion.

## References

[1] J. Bekaert, A. Aperis, B. Partoens, P. M. Oppeneer, M. V. Milošević, Advanced first-principles theory of superconductivity including both lattice vibrations and spin fluctuations: The case of $FeB_4$, Phys. Rev. B 97 (2018) 014503. doi:10.1103/PhysRevB.97.014503.

[2] G. Ghigo, D. Torsello, G. A. Ummarino, L. Gozzelino, M. A. Tanatar, R. Prozorov, P. C. Canfield, Disorder-driven transition from $s_{\pm}$ to $s_{++}$ superconducting order parameter in proton irradiated $Ba(Fe_{1-x}Rh_x)_2As_2$ single crystals, Phys. Rev. Lett. 121 (2018) 107001. doi:10.1103/PhysRevLett.121.107001.

[3] D. Torsello, G. A. Ummarino, R. Gerbaldo, L. Gozzelino, G. Ghigo, Eliashberg analysis of the electrodynamic response of $Ba(Fe_{1-x}Rh_x)_2As_2$ across the $s_{\pm}$ to $s_{++}$ order parameter transition, J. Supercond. Nov. Magn. 33 (2020) 2319â2324. doi:10.1007/s10948-019-05368-2.

[4] F. Schrodi, A. Aperis, P. M. Oppeneer, Eliashberg theory for spin fluctuation mediated superconductivity: Application to bulk and monolayer FeSe, Phys. Rev. B 102 (2020) 014502. doi:10.1103/PhysRevB.102.014502.

[5] R. Khasanov, Z. Guguchia, Probing the multi gap behavior within '11' and '122' families of iron based superconductors: the muon-spin rotation studies, Superconductor Science and Technology 28 (3) (2015) 034003. doi:10.1088/0953-2048/28/3/034003.

[6] I. Mazin, J. Schmalian, Pairing symmetry and pairing state in ferropnictides: Theoretical overview, Physica C 469 (9) (2009) 614 – 627. doi:https://doi.org/10.1016/j.physc.2009.03.019.

[7] M. M. Korshunov, Superconducting state in iron-based materials and spin-fluctuation pairing theory, Physics-Uspekhi 57 (8) (2014) 813–819. doi:10.3367/ufne.0184.201408h.0882.

[8] H. Hosono, K. Kuroki, Iron-based superconductors: Current status of materials and pairing mechanism, Physica C: Superconductivity and its Applications 514 (2015) 399 – 422. doi:https://doi.org/10.1016/j.physc.2015.02.020.

[9] H.-H. Kuo, J.-H. Chu, J. C. Palmstrom, S. A. Kivelson, I. R. Fisher, Ubiquitous signatures of nematic quantum criticality in optimally doped Fe-based superconductors, Science 352 (6288) (2016) 958–962. doi:10.1126/science.aab0103.

[10] P. J. Hirschfeld, M. M. Korshunov, I. I. Mazin, Gap symmetry and structure of Fe-based superconductors, Rep. Prog. Phys. 74 (12) (2011) 124508.

[11] D. Torsello, R. Gerbaldo, L. Gozzelino, M. A. Tanatar, R. Prozorov, P. C. Canfield, G. Ghigo, Electrodynamic response of Ba $(Fe_{1-x}Rh_x)_2As_2$ across the s± to $s_{++}$ order parameter transition, The European Physical Journal Special Topics 228 (3) (2019) 719–723. doi:10.1140/epjst/e2019-800144-1.

[12] H. Ding, P. Richard, K. Nakayama, K. Sugawara, T. Arakane, Y. Sekiba, A. Takayama, S. Souma, T. Sato, T. Takahashi, Z. Wang, X. Dai, Z. Fang, G. F. Chen, J. L. Luo, N. L. Wang, Observation of fermi-surface–dependent nodeless superconducting gaps in $Ba_{0.6}K_{0.4}Fe_2As_2$, EPL (Europhysics Letters) 83 (4) (2008) 47001. doi:10.1209/0295-5075/83/47001.

[13] D. Wu, W. Hong, C. Dong, X. Wu, Q. Sui, J. Huang, Q. Gao, C. Li, C. Song, H. Luo, C. Yin, Y. Xu, X. Luo, Y. Cai, J. Jia, Q. Wang, Y. Huang, G. Liu, S. Zhang, F. Zhang, F. Yang, Z. Wang, Q. Peng, Z. Xu, X. Qiu, S. Li, H. Luo, J. Hu, L. Zhao, X. J. Zhou, Spectroscopic evidence of bilayer splitting and strong interlayer pairing in the superconductor $KCa_2Fe_4As_4F_2$, Phys. Rev. B 101 (2020) 224508. doi:10.1103/PhysRevB.101.224508.

[14] G. Wang, Z. Wang, X. Shi, Self-hole-doping–induced superconductivity in $KCa_2Fe_4As_4F_2$, EPL (Europhysics Letters) 116 (3) (2016) 37003. doi:10.1209/0295-5075/116/37003.

[15] A. Ghosh, S. Ghosh, H. Ghosh, Electron correlation induced orbital selective lifshitz transition in new hybrid 12442 iron based superconductors, Computational Materials Science 183 (2020) 109802.

[16] M. Smidman, F. K. K. Kirschner, D. T. Adroja, A. D. Hillier, F. Lang, Z. C. Wang, G. H. Cao, S. J. Blundell, Nodal multigap superconductivity in $KCa_2Fe_4As_4F_2$, Phys. Rev. B 97 (2018) 060509. doi:10.1103/PhysRevB.97.060509.

[17] T. Wang, J. Chu, J. Feng, L. Wang, X. Xu, W. Li, H. Wen, X. Liu, G. Mu, Low temperature specific heat of 12442-type $KCa_2Fe_4As_4F_2$ single crystals, SCIENCE CHINA Physics, Mechanics & Astronomy 63 (2020) 1–6.

[18] Z.-C. Wang, C.-Y. He, S.-Q. Wu, Z.-T. Tang, Y. Liu, A. Ablimit, C.-M. Feng, G.-H. Cao, Superconductivity in $KCa_2Fe_4As_4F_2$ with separate double $Fe_2As_2$ layers, Journal of the American Chemical Society 138 (25) (2016) 7856–7859. doi:10.1021/jacs.6b04538.

[19] X. Yi, M. Li, X. Xing, Y. Meng, C. Zhao, Z. Shi, Single crystal growth and effects of ni doping on the novel 12442-type iron-based superconductor $RbCa_2Fe_4As_4F_2$, New Journal of Physics 22 (7) (2020) 073007. doi:10.1088/1367-2630/ab9427.

[20] X. Xing, X. Yi, M. Li, Y. Meng, G. Mu, J.-Y. Ge, Z. Shi, Vortex phase diagram in 12442-type $RbCa_2Fe_4As_4F_2$ single crystal revealed by magneto-transport and magnetization measurements, Superconductor Science and Technology 33 (11) (2020) 114005. doi:10.1088/1361-6668/abb35f.
URL `https://doi.org/10.1088/1361-6668/abb35f`

[21] W. Hong, L. Song, B. Liu, Z. Li, Z. Zeng, Y. Li, D. Wu, Q. Sui, T. Xie, S. Danilkin, H. Ghosh, A. Ghosh, J. Hu, L. Zhao, X. Zhou, X. Qiu, S. Li, H. Luo, Neutron spin resonance in a quasi-two-dimensional iron-based superconductor, Phys. Rev. Lett. 125 (2020) 117002. doi:10.1103/PhysRevLett.125.117002.

[22] S. Pyon, Y. Kobayashi, A. Takahashi, W. Li, T. Wang, G. Mu, A. Ichinose, T. Kambara, A. Yoshida, T. Tamegai, Anisotropic physical properties and large critical current density in $KCa_2Fe_4As_4F_2$ single crystal, Phys. Rev. Materials 4 (2020) 104801. doi:10.1103/PhysRevMaterials.4.104801.

[23] T. Wang, C. Zhang, L. Xu, J. Wang, S. Jiang, Z. Zhu, Z. Wang, J. Chu, J. Feng, L. Wang, et al., Strong pauli paramagnetic effect in the upper critical field of $KCa_2$ $Fe_4As_4F_2$, SCIENCE CHINA Physics, Mechanics & Astronomy 63 (2) (2020) 1–6.

[24] E. Gati, L. Xiang, S. L. Bud'ko, P. C. Canfield, Hydrostatic and uniaxial pressure tuning of iron-based superconductors: Insights into superconductivity, magnetism, nematicity, and collapsed tetragonal transitions, Annalen der Physik 532 (10) (2020) 2000248. doi:https://doi.org/10.1002/andp.202000248.

[25] G. Ghigo, D. Torsello, L. Gozzelino, T. Tamegai, I. S. Veshchunov, S. Pyon, W. Jiao, G.-H. Cao, S. Y. Grebenchuk, I. A. Golovchanskiy, V. S. Stolyarov, D. Roditchev, Microwave analysis of the interplay between magnetism and superconductivity in $EuFe_2(As_{1-x}P_x)_2$ single crystals, Phys. Rev. Research 1 (2019) 033110. doi:10.1103/PhysRevResearch.1.033110.

[26] G. Ummarino, Phenomenology of $CaKFe_4As_4$ explained in the framework of four bands eliashberg theory, Physica C: Superconductivity and its Applications 529 (2016) 50 – 53. doi:https://doi.org/10.1016/j.physc.2016.09.002.

[27] D. Torsello, G. A. Ummarino, L. Gozzelino, T. Tamegai, G. Ghigo, Comprehensive eliashberg analysis of microwave conductivity and penetration depth of K-, Co-, and P-substituted $BaFe_2As_2$, Phys. Rev. B 99 (2019) 134518. doi:10.1103/PhysRevB.99.134518.

[28] D. Torsello, K. Cho, K. R. Joshi, S. Ghimire, G. A. Ummarino, N. M. Nusran, M. A. Tanatar, W. R. Meier, M. Xu, S. L. Bud'ko, P. C. Canfield, G. Ghigo, R. Prozorov, Analysis of the London penetration depth in Ni-doped $CaKFe_4As_4$, Phys. Rev. B 100 (2019) 094513. doi:10.1103/PhysRevB.100.094513.

[29] G. A. Ummarino, D. Daghero, Possible mixed coupling mechanism in $FeTe_{1-x}Se_x$within a multiband eliashberg approach, Journal of Physics: Condensed Matter 27 (43) (2015) 435701. doi:10.1088/0953-8984/27/43/435701.

[30] A. A. Golubov, O. V. Dolgov, A. Boris, A. Charnukha, D. Sun, C. Lin, A. Shevchun, A. Korobenko, M. R. Trunin, V. N. Zverev, Normal state resistivity of $Ba_{1-x}K_xFe_2As_2$: evidence for multiband strong-coupling behavior, JETP letters 94 (4) (2011) 333–337.

[31] P. Popovich, A. V. Boris, O. V. Dolgov, A. A. Golubov, D. L. Sun, C. T. Lin, R. K. Kremer, B. Keimer, Specific heat measurements of $Ba_{0.68}K_{0.32}Fe_2As_2$ single crystals: Evidence for a multiband strong-coupling superconducting state, Phys. Rev. Lett. 105 (2010) 027003. doi:10.1103/PhysRevLett.105.027003.

[32] G. Eliashberg, Interactions between electrons and lattice vibrations in a superconductor, Sov. Phys. JETP 11 (3) (1960) 696–702.

[33] G. A. Ummarino, Multiband $s\pm$ eliashberg theory and temperature-dependent spin-resonance energy in iron pnictide superconductors, Phys. Rev. B 83 (2011) 092508. doi:10.1103/PhysRevB.83.092508.

[34] D. Inosov, J. Park, P. Bourges, D. Sun, Y. Sidis, A. Schneidewind, K. Hradil, D. Haug, C. Lin, B. Keimer, et al., Normal-state spin dynamics and temperature-dependent spin-resonance energy in optimally doped $BaFe_{1.85}Co_{0.15}As_2$, Nature Physics 6 (3) (2010) 178.

[35] L. Boeri, M. Calandra, I. I. Mazin, O. V. Dolgov, F. Mauri, Effects of magnetism and doping on the electron-phonon coupling in $BaFe_2As_2$, Phys. Rev. B 82 (2010) 020506. doi:10.1103/PhysRevB.82.020506.

[36] I. I. Mazin, D. J. Singh, M. D. Johannes, M. H. Du, Unconventional superconductivity with a sign reversal in the order parameter of $LaFeAsO_{1-x}F_x$, Phys. Rev. Lett. 101 (2008) 057003. doi:10.1103/PhysRevLett.101.057003.

[37] M. Tortello, D. Daghero, G. A. Ummarino, V. A. Stepanov, J. Jiang, J. D. Weiss, E. E. Hellstrom, R. S. Gonnelli, Multigap superconductivity and strong electron-boson coupling in fe-based superconductors: A point-contact andreev-reflection study of $Ba(Fe_{1-x}Co_x)_2As_2$ single crystals, Phys. Rev. Lett. 105 (2010) 237002. doi:10.1103/PhysRevLett.105.237002.

[38] G. Ghigo, G. A. Ummarino, L. Gozzelino, T. Tamegai, Penetration depth of $Ba_{1-x}K_xFe_2As_2$ single crystals explained within a multiband eliashberg $s\pm$ approach, Phys. Rev. B 96 (2017) 014501. doi:10.1103/PhysRevB.96.014501.

[39] C. Zhang, T. Hu, T. Wang, Y. Wu, A. Yu, J. Chu, H. Zhang, H. Xiao, W. Peng, Z. Di, S. Qiao, G. Mu, Observation of two-dimensional superconductivity in an ultrathin iron-arsenic superconductor (2020). arXiv:2006.03338.

[40] H. Suderow, V. G. Tissen, J. P. Brison, J. L. Martínez, S. Vieira, P. Lejay, S. Lee, S. Tajima, Pressure dependence of the upper critical field of $MgB_2$ and of $YNi_2B_2C$, Phys. Rev. B 70 (2004) 134518. doi:10.1103/PhysRevB.70.134518.

[41] G. Ghigo, G. A. Ummarino, L. Gozzelino, R. Gerbaldo, F. Laviano, D. Torsello, T. Tamegai, Effects of disorder induced by heavy-ion irradiation on $(Ba_{1-x}K_x)Fe_2As_2$ single crystals, within the three-band Eliashberg $s_\pm$ wave model, Sci. Rep. 7 (1) (2017) 13029.
URL `http://www.nature.com/articles/s41598-017-13303-5`

[42] D. Torsello, G. Ummarino, J. Bekaert, L. Gozzelino, R. Gerbaldo, M. Tanatar, P. Canfield, R. Prozorov, G. Ghigo, Tuning the intrinsic anisotropy with disorder in the $CaKFe_4As_4$ superconductor, Phys. Rev. Applied 13 (2020) 064046. doi:10.1103/PhysRevApplied.13.064046.

[43] L. Benfatto, E. Cappelluti, C. Castellani, Spectroscopic and thermodynamic properties in a four-band model for pnictides, Phys. Rev. B 80 (2009) 214522. doi:10.1103/PhysRevB.80.214522.

[44] F. K. K. Kirschner, D. T. Adroja, Z.-C. Wang, F. Lang, M. Smidman, P. J. Baker, G.-H. Cao, S. J. Blundell, Two-gap superconductivity with line nodes in $CsCa_2Fe_4As_4F_2$, Phys. Rev. B 97 (2018) 060506. doi:10.1103/PhysRevB.97.060506.

[45] P. B. Allen, New method for solving boltzmann's equation for electrons in metals, Phys. Rev. B 17 (1978) 3725–3734. doi:10.1103/PhysRevB.17.3725.

[46] G. Grimvall, et al., The electron-phonon interaction in metals (1981).

[47] P. B. Allen, B. Chakraborty, Infrared and dc conductivity in metals with strong scattering: Nonclassical behavior from a generalized boltzmann equation containing band-mixing effects, Phys. Rev. B 23 (1981) 4815–4827. doi:10.1103/PhysRevB.23.4815.

[48] E. Maksimov, M. Kulić, O. Dolgov, Bosonic spectral function and the electron-phonon interaction in htsc cuprates, Advances in Condensed Matter Physics 2010 (2010).

[49] G. A. Ummarino, S. Galasso, P. Pecchio, D. Daghero, R. S. Gonnelli, F. Kurth, K. Iida, B. Holzapfel, Resistivity in Ba(FeCo)As: Comparison of thin films and single crystals, physica status solidi (b) 252 (4) (2015) 821–827. doi:https://doi.org/10.1002/pssb.201451460.

[50] A. Charnukha, O. V. Dolgov, A. A. Golubov, Y. Matiks, D. L. Sun, C. T. Lin, B. Keimer, A. V. Boris, Eliashberg approach to infrared anomalies induced by the superconducting state of $Ba_{0.68}K_{0.32}Fe_2As_2$ single crystals, Phys. Rev. B 84 (2011) 174511. doi:10.1103/PhysRevB.84.174511.

[51] Y. A. Aleshchenko, A. V. Muratov, G. A. Ummarino, S. Richter, A. A. Thomas, R. HÃ¼hne, Optical and hidden transport properties of $BaFe_{1.91}Ni_{0.09}As_2$ film, Journal of Physics: Condensed Matter 33 (4) (2020) 045601. doi:10.1088/1361-648x/abbc33.